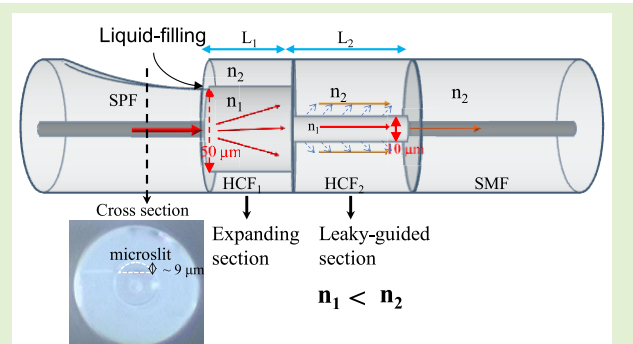


Effective Liquid-Filled Leaky-Guided Fiber Mach–Zehnder Interferometer With a Side-Polished Fiber

Cheng-Ling Lee^{ID}, Chun-Yu Yeh, and Yu-Xin Jiang

Abstract—We first propose an effective liquid-filled leaky-guided fiber Mach–Zehnder interferometer (LGFMZI) utilizing a side-polished fiber (SPF) for high-sensitivity liquid material sensing. The structure features a side-polished single-mode fiber (SMF) sequentially spliced to large-core (HCF_1) and small-core hollow-core fibers (HCF_2), with a terminal SMF segment. The SPF, connected to HCF_1 , forms a microslit that facilitates effective liquid injection into HCF_2 . In the design, the refractive index (RI) of the liquid (n_1), being lower than that of the silica cladding (n_2), induces a leaky-guided (LG) fiber waveguide in the tiny HCF_2 section, enabling the core and cladding modes generation. HCF_1 functions as a beam splitter, expanding the light into the core of HCF_2 and cladding to balance their intensities, thereby enhancing the interference extinction ratio (ER). Experimental results demonstrate that high sensitivity of $11.93 \text{ nm}/^\circ\text{C}$ and an ER exceeding 30 dB with a tunable free spectral range (FSR) of interference spectra are achieved by adjusting the lengths of HCF_1 and HCF_2 . Furthermore, the interference spectra exhibit a linear thermal response across an ultrawide wavelength range (1250–1650 nm), offering significant advantages for sensing applications.

Index Terms—Fiber Mach–Zehnder interferometer (FMZI), fiber-optic sensors, leaky-guided (LG), side-polished fiber (SPF).



I. INTRODUCTION

HOLLOW-CORE fibers (HCFs) have attracted considerable attention in recent years due to their hollow central core structure, which allows for the accommodation of various specimens such as liquids [1], [2], [3], [4], gases [5], and polymers [6], [7]. This feature provides more significant development potential compared to solid-core optical fibers. HCFs can be classified into photonic crystal fibers (PCFs) and capillary optical fibers (COFs). PCFs exhibit unique and advantageous properties due to the periodic air hole structure in the cladding region. They are considered promising optical fiber structures with large birefringence, high-temperature (T) stability, controllable sensitivity, and significant flexibility in fiber waveguide design. To date, a range of functional optical fiber devices have been developed by infusing the air holes of

PCFs with liquid or other materials to induce desired optical effects: compact fiber polarizers [8], tunable photonic bandgap fiber passive devices [9], and optical fiber sensors [10], [11], [12], [13]. However, the challenges of PCFs for fabrication mainly include: 1) maintaining the air holes at a specific size and position of indifferent rings and 2) precisely controlling the T and the drawing speed during the drawing process to prevent the collapsing of the air holes [14]. In summary, the structure of PCFs makes their fabrication more complex and costly than traditional fibers, which prevents their widespread application. Therefore, the straightforward structure and low manufacturing cost of COFs render them a more favorable option. COF is a simple glass structure that utilizes the antiresonant reflecting mechanism from the inner and outer walls, allowing light to propagate through the air core [15]. Capillary fibers are used in various sensing fields, including the refractive index (RI) [16], temperature (T) [17], [18], [19], [20], [21], liquid level [22], pressure [23], thermal optics coefficient (TOC) [24], [25], relative humidity [26], and magnetic field strength [21].

Recently, many techniques have been developed to facilitate the sample's introduction into the core of the HCF. For instance, in 2019, Liu et al. [16] developed a simple fiber sensor based on the COF to measure both the RI and T simultaneously. The method for this optical fiber sensor

Received 7 December 2024; accepted 20 January 2025. Date of publication 11 February 2025; date of current version 14 March 2025. This work was supported by the Ministry of Science and Technology of Taiwan under Grant MOST 110-2221-E-239-025-MY2. The associate editor coordinating the review of this article and approving it for publication was Dr. Antreas Theodosiou. (Corresponding author: Cheng-Ling Lee.)

The authors are with the Department of Electro-Optical Engineering, National United University, Miaoli 36003, Taiwan (e-mail: cherry@nuu.edu.tw; U1023040@o365.nuu.edu.tw; U1023008@o365.nuu.edu.tw).

Digital Object Identifier 10.1109/JSEN.2025.3538788

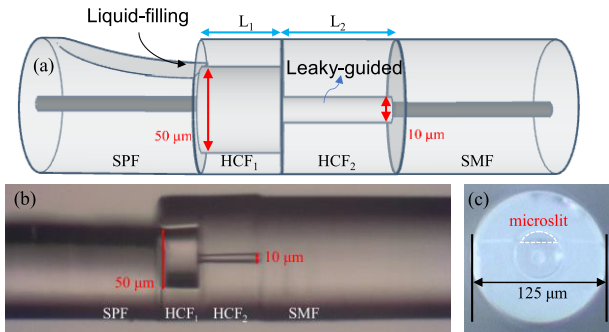


Fig. 1. (a) Configuration of the proposed LGFMZI with the SPF. (b) Micrograph of the proposed sensor structure. (c) Microscopic image of the cross section of HCF₁.

involves using capillary action to fill the hollow core and then splicing the infiltrated fiber into single-mode fibers (SMFs) at both ends to retain the liquid within the core. However, it is important to note that this approach may lead to evaporation during the fusion splicing process, potentially leaving a section of the unfilled area near the joint, consequently resulting in a low T sensitivity of only $-42.7 \text{ pm}^{\circ}\text{C}$. In 2020, Lee et al. [24] proposed a microhole-pair HCF Fabry–Perot interferometer. They achieved quick liquid access to the HCF by symmetrically microdrilling two microholes in the sidewall of the fiber using a femtosecond (fs) laser micromachining technique. However, the fabrication of microholes requires high precision and stability of the stage in the machining system. Due to the substantial expense and complex maintenance needs of the fs laser, this manufacturing method is not widely adopted. An ultracompact leaky-guided (LG) liquid-core fiber Mach–Zehnder interferometer (LLCFMZI) was presented in 2022. The sensor structure is based on a micro-sized HCF splicing a tilted endface SMF to create a miniature oblique gap to access different liquids effectively [27]. However, the proposed LLCFMZI is easy breakage because it utilizes slant cleaving on the SMF endface, and it needs tiny core-offset splicing to achieve a good extinction ratio (ER) of interference. In 2024, Lu et al. [28] proposed a novel LG FMZI based on connections of two discrepant HCFs to improve these limitations. The FMZI structure is based on a tiny HCF with a small diameter of 10 μm, connected to a larger-core HCF as a beam splitter to expand the optical beam. By precisely adjusting the lengths of both HCFs, it can perform ultrahigh ER, ultracompact, and broadband interference characteristics. The fiber interferometer configuration can achieve an ultrahigh ER exceeding 50 dB, with an arbitrary free spectral range (FSR) in the transmitted interference spectra over an extensive wavelength range of 1250–1650 nm [28]. Nevertheless, this method cannot allow for the measurement of the properties of the materials in the HCF.

In this article, we presented an effective liquid-filled leaky-guided fiber Mach–Zehnder interferometer (LGFMZI) assisted by a side-polished fiber (SPF) capable of sensing liquid materials with high sensitivity. The structure consists of a side-polished SMF sequentially spliced to large- and small-core hollow-core fibers (HCFs), followed by a final segment of the SMF. The proposed SPF connected to the large-core HCF (HCF₁) can create a microslit to effectively access liquids

into the small-core HCF (HCF₂). Specifically, HCF₁ also serves as a beam splitter and balances the cladding and core modes' intensities of HCF₂ to achieve a better ER of the interference. Experimental results showing a high sensitivity of 11.93 nm/°C and a high ER over 30 dB with arbitrary spectra of interference can be achieved by adjusting the lengths of HCF₁ and HCF₂. The results also show that the interference spectra linearly respond to thermal effect. They also can achieve a single-wavelength dip over an ultrawide wavelength measurement range, making it a wideband tunable optical fiber filter.

II. FABRICATION AND PRINCIPLE

The proposed LGFMZI with the SPF is elaborately designed as follows: Initially, a segment of HCF₁ with a diameter of 50 μm is fusion-spliced to a prefabricated SPF to create a microslit. This microslit serves as a critical interface for liquid filling. The opposite end of HCF₁ is then fusion-spliced with another segment of HCF₂, which has a smaller diameter of 10 μm. Finally, HCF₂ is fusion-spliced to another segment of the SMF, forming the complete optical waveguide device. In this structure, the lengths of HCF₁ and HCF₂ are referred to as L₁ and L₂, respectively. The detailed structure is illustrated in Fig. 1. In this experimental setup, the presence of a microslit between HCF₁ and the polished SMF allows for capillary action to effectively fill the cores of both HCF₁ and HCF₂ with the sample. This innovative approach utilizes polishing and fusion splicing techniques under carefully controlled parameters, resulting in a method that is not only cost-effective but also facilitates easy fabrication.

Fig. 2 depicts the experimental setup for measuring the thermal characteristics of the LGFMZI. The measurement system comprises an optical spectrum analyzer (OSA, ADVANTEST-Q8381A) and a broadband light source (BLS) that operates within the wavelengths of 1250–1650 nm. As the light from the BLS propagates through the SPF and into HCF₁, it disperses within the large hollow core. Due to the LG fiber waveguide phenomenon, the light gradually separates into two distinct portions as it propagates through HCF₂, with each beam propagating through either the silica cladding or the leaky liquid core. These two beams subsequently recombine at the HCF₂ end, resulting in superimposed. An output SMF is employed to collect the optical signals for measurement. In summary, the optical response of the LGFMZI is characterized by the interference of two beams: one from the cladding mode and the other from the leaky guided core mode, effectively achieving such a tiny all-fiber FMZI configuration that produces a sinusoidal interference pattern over the broad wavelength range.

The optical intensities of the cladding and core beams within HCF₂ in the proposed SPF LGFMZI (SPF-LGFMZI) structure are denoted as I_{co} and I_{cl}, respectively, while the total intensity of the interference beam, represented as I, is defined by

$$I = I_{\text{co}} + I_{\text{cl}} + \sqrt{I_{\text{co}} \cdot I_{\text{cl}}} \cos\left(\frac{2\pi}{\lambda} \Delta n^{\text{eff}} L_2\right) \quad (1)$$

where $\Delta n^{\text{eff}} = |n_{\text{co}}^{\text{eff}} - n_{\text{cl}}^{\text{eff}}|$ is the effective index difference between cladding ($n_{\text{cl}}^{\text{eff}}$) and core modes ($n_{\text{co}}^{\text{eff}}$). λ denotes the

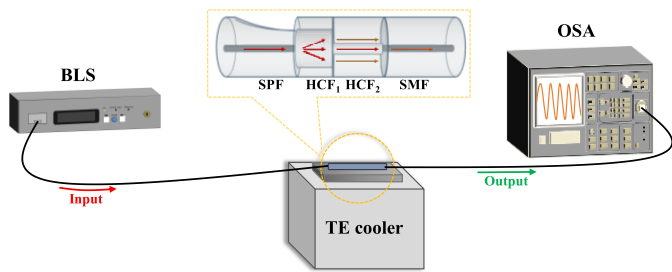


Fig. 2. Schematic of the experimental setup for the SPF-LGFMZI.

wavelength of the light. When the optical phase difference ($(2\pi/\lambda)\Delta n^{\text{eff}} \cdot L_2$) conforms to the condition of destructive interference, the dip wavelength of minimum power (λ_{\min}^m) can be deduced as

$$\lambda_{\min}^m = \frac{2}{2m+1} \Delta n^{\text{eff}} L_2. \quad (2)$$

Here, m is the order of the interferential mode and it is an integer. The FSR of the interferometers means the wavelength difference of two continuous interference dips or peaks between the front and the rear. Afterward, we can utilize the relationship of interference phase difference to obtain the FSR, which can be expressed as

$$\text{FSR} = |\lambda_1 - \lambda_2| = \frac{\lambda_1 \lambda_2}{|n_{\text{co}}^{\text{eff}} - n_{\text{cl}}^{\text{eff}}| L_2} \quad (3)$$

where λ_1 and λ_2 represent the wavelengths of two adjacent interference dips. $n_{\text{co}}^{\text{eff}}$ and $n_{\text{cl}}^{\text{eff}}$ are the effective RI of the cladding and core modes in the interference.

III. EXPERIMENTAL RESULTS AND DISCUSSION

Two different configurations were performed and measured to investigate the impact of the used HCF₁ on the interference spectra of our designed sensor. The first structure, SMF–HCF₂–SMF, is based on the fusion-splicing of the SMF at both ends, incorporating HCF₂, with L_2 of HCF₂ being 30.5 μm. On the other hand, the second structure, designated as SMF–HCF₁–HCF₂–SMF, consists of HCF₁ fused with HCF₂, followed by fusion splicing with the SMF at both ends, where L_1 of HCF₁ is round 93.0 μm, while L_2 of HCF₂ remains 30.5 μm. The LG waveguide means the filled liquid whose RI is lower than that of the silica cladding. It gradually causes the core light to leak into the cladding along HCF₂. As illustrated in Fig. 3, the first configuration's ER is notably lower than that of the second structure while their FSRs are similar due to the same HCF₂. It is attributed to the fact that the SMF–HCF₂–SMF configuration does not achieve a significant interference length, leading to a shallower ER of only 12.15 dB, compared to the ER of the interference spectrum in the SMF–HCF₁–HCF₂–SMF configuration, which reaches a value of 28.41 dB. Conversely, the SMF–HCF₁–HCF₂–SMF configuration demonstrates an advanced design with a deeper ER. It is approximately 2.33 times greater than that in the SMF–HCF₂–SMF design. This significant improvement is primarily due to the incorporation of HCF₁, which effectively assists in splitting the optical light into core and cladding beams that are subsequently launched into the

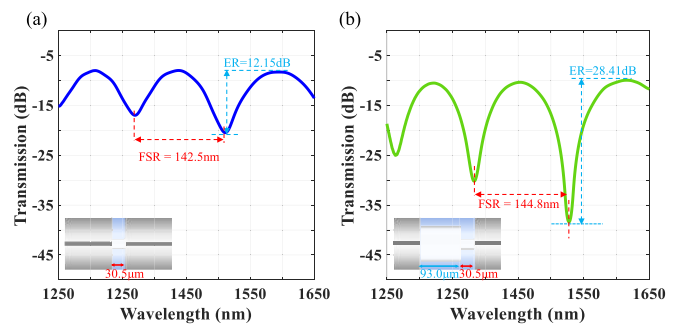


Fig. 3. Optical interference spectra of the proposed SPF-LGFMZI (a) without the segment of HCF₁ and (b) with the segment of HCF₁. Insets individually show their structures.

leaky HCF₂ with appropriate intensities. In summary, HCF₁'s role in enhancing the ER performance of the interferometer is crucial.

Fig. 4 illustrates the interference spectra of the proposed interferometers with different HCF₁ and HCF₂ arrangement lengths. Notably, the corresponding lengths of L_1 are 116.5, 40.1, 40.3, 48.2, 37.0, and 78.9 μm when the connected HCF₂ with L_2 is 22.1, 35.2, 64.2, 66.2, 88.6, and 91.1 μm, respectively. The observations in Fig. 4(a)–(f) reveal a key role: as L_2 increases from 22.1 to 91.1 μm, the FSR decreases from 198.4 to 44.8 nm. This inverse relationship between L_2 and FSR, as indicated by (3), is a significant finding. It suggests that HCF₂ primarily contributes to the region-of-light interference; on the other hand, the varying length of HCF₁ serves a specific function as a beam splitter or beam expander in the designed structure. This emphasis on the role of HCF₁ informs us about its function in the designed interferometer. Consequently, the length of L_1 only influences the ER of the interference spectra and does not affect the FSR of the interference spectra.

Furthermore, upon examining the thickness of the SPF fused to HCF₁ and the length of HCF₂ to the corresponding spectral losses, it becomes apparent that a thinner-diameter SPF or a longer HCF₂ results in higher interference losses. One can see in the cases of Fig. 4(a), (b), and (f) that longer HCF₂ has greater loss with the thickness of the SPFs similar to around 80 μm. In two similar cases in the results of Fig. 4(c) and (d), the thickness of the SPFs approaches 72–73 μm/ L_2 around 64–66 μm, and the associated spectral losses are around 20 dB. On the other hand, in Fig. 4(e) and (f), the SPFs are thicker near 80 μm, and a high loss of about 20 dB also can be observed since the longer L_2 than those of the conditions in Fig. 4(c) and (d). The phenomenon occurs because the evanescent wave reduces optical light from the SPFs and the leaky features by the long-waveguide HCF₂. Therefore, in our designed aim, the current effective method is to prevent too thin SPF when L_2 is fixed which can improve spectral transmission.

To investigate the dynamics of liquid filling in the two connected HCFs' structures via the used SPF, we employed [®]Cargille optical liquid with an RI of $n_D = 1.35$ to illustrate this process. The unique design of HCF₁, which is fusion-spliced to a side-polished SMF, facilitates the creation

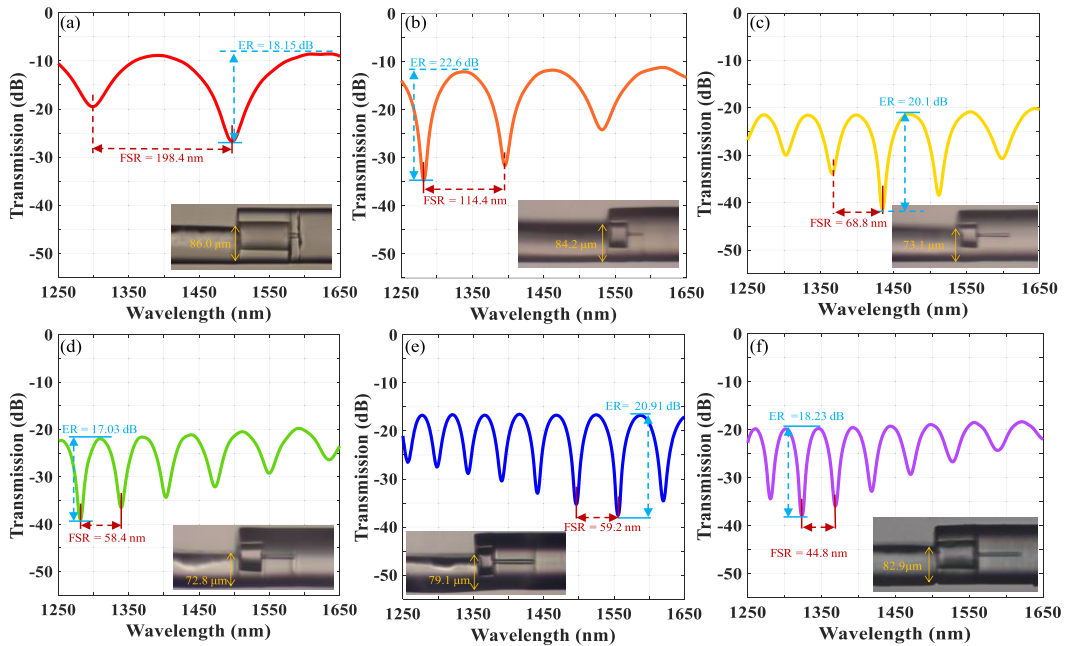


Fig. 4. Interference spectra obtained from the designed interferometer (air core) under different lengths of HCF₁ and HCF₂ with the SPF thickness of (a) 86.0 μm , (b) 84.2 μm , (c) 73.1 μm , (d) 72.8 μm , (e) 79.1 μm , and (f) 82.9 μm .

of a microslit. This configuration allows direct liquid access and enhances the interaction between the liquid and HCFs. The filling mechanism is primarily driven by the liquid's adhesive forces and surface tension, which generates a significant capillary effect within the hollow core of HCFs. This capillary action enables the liquid to ascend into the core, filling it over time. Fig. 5(a)–(e) illustrates a series of microphotographs documenting the gradual filling of the HCFs with the filled liquid from the microslit. Their corresponding temporal evolutions of the interference spectra are captured and plotted in Fig. 5(f)–(j), highlighting the changes in optical characteristics as the liquid progressively fills the HCFs. Each spectrum reflects the dynamic interaction between the light and the varying liquid volume, providing insights into the optical behavior during the filling process. As the liquid occupies more of HCF₁, we observe a noticeable increase in the filled area, which correlates with alterations in the interference patterns. This phenomenon can be attributed to the presence of liquid within HCF₁ modifying the optical path length during beam expansion, impacting the ER associated with the optical interference performance. Also, it is important to note that the FSR remains nearly constant as long as the liquid has not infiltrated HCF₂, as shown in Fig. 5(f)–(h). However, once the liquid infiltrates HCF₂, the FSR and ER of the interference spectrum undergo significant changes, driven by the interaction between the core mode and the cladding mode. Ultimately, when two HCFs are filled, the optical spectra will stabilize and remain unchanged. It can be seen that once HCF₂ is filled with the liquids, the FSR significantly increases. The LG mechanism can be achieved when the HCF₂ core is filled with a liquid with an RI lower than the cladding.

According to the experimental results, the proposed interferometer can effectively vary different interference wavelength dips over a broadband wavelength range with good interference performance by precisely adjusting the lengths of HCF₁

and HCF₂ and by introducing liquid as the core materials. This adjustment also makes an interference wavelength dip with exceptionally high ER, as shown in Fig. 6(a)–(c). Notably, the insertion loss is around -10 dB for the various combinations of HCF₁/HCF₂ filled with the Cargille liquids ($n_{\text{D}} = 1.30$). Subsequently, the device was heated, with the temperature (T) incrementally increased from 25 °C to 45 °C to investigate the impact of thermal variations on the interference spectra. The results demonstrate that the spectral wavelength shifts ($\Delta\lambda$) toward longer wavelengths as T increases and exhibits extremely linear responses and steady characteristics. This situation can be understood by the following T-sensitivity ($S \equiv \Delta\lambda/\Delta T$) equation [27]:

$$S = \lambda \left(\frac{k_{\text{cl}} \cdot n_{\text{cl}}^{\text{eff}}(T) - k_{\text{co}} \cdot n_{\text{co}}^{\text{eff}}(T)}{n_{\text{cl}}^{\text{eff}}(T) - n_{\text{co}}^{\text{eff}}(T)} \right) \quad (4)$$

where k_{cl} is the TOC for the silica cladding of the fiber ($\text{TOC} = +10.5^\circ \times 10^{-6} \text{ }^\circ\text{C}^{-1}$) and k_{co} is TOC for the optical liquid ($\text{TOC} = (dn_{\text{D}}/dt)/n_{\text{D}} = (-3.33/1.3) \times 10^{-4} \text{ }^\circ\text{C}^{-1}$ for $n_{\text{D}} = 1.3$) [29]. λ is the monitoring wavelength dip. $n_{\text{co}}^{\text{eff}}(T)$ and $n_{\text{cl}}^{\text{eff}}(T)$ are the effective indices of the liquid core and silica cladding at a specific T , respectively. Based on the theoretical relationship described by (4), the T-sensitivity of the proposed SPF-LGFMZI increases as the liquid's RI approaches the cladding RI. In (4), $n_{\text{cl}}^{\text{eff}}(T) - n_{\text{co}}^{\text{eff}}(T)$ is positive, and k_{co} is typically negative. Consequently, the S values are positive, meaning the interference wavelengths shifted to longer wavelengths. The corresponding sensitivities (S) of the different structures of the sensors shown in Fig. 6(d)–(f) are measured at 3.54, 3.44, and 3.32 nm/°C across an ultrabroad wavelength range, respectively. We further calculate the theoretical values using (4) to obtain the corresponding S , which are 3.30, 3.64, and 3.45 nm/°C, by their monitoring wavelength dip of 1430.8, 1566.8, and 1486.8 nm at 25 °C, respectively. It is

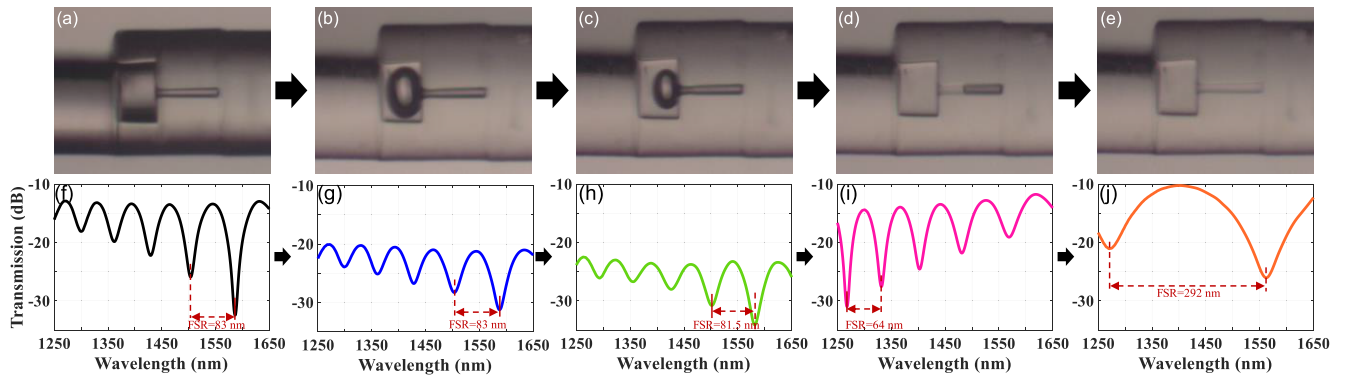


Fig. 5. (a)–(e) Evolutions of microphotographs of the Cargille liquid ($n_D = 1.35$) filling to L_1/L_2 of $40.7/64.6 \mu\text{m}$. (f)–(j) Duration corresponding to optical spectra, respectively.

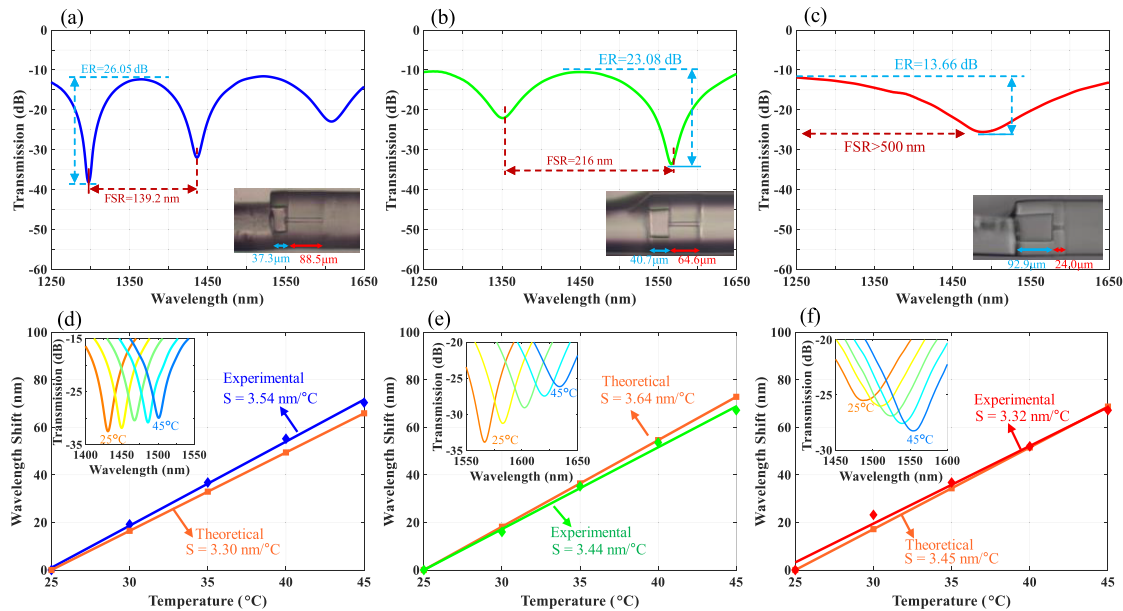


Fig. 6. (a)–(c) Interference spectra corresponding to the SPF-LGFMZI of the different lengths of HCF₁ and HCF₂ with the filled-liquid Cargille liquid ($n_D = 1.30$). (d)–(f) Corresponding T-sensitivities of the wavelength shift from 25 °C to 45 °C for the cases of (a)–(c).

noteworthy that the experimental results have agreement with the theoretical results.

To study the impacts of the SPF-LGFMZI under conditions involving the HCF core with different RIs, a series of liquids were systematically tested to evaluate the FSR and ER of the interference spectra. Fig. 7(a)–(e) illustrates the measured interference spectra for the Cargille liquids of $n_D = 1.30$, 1.35, and 1.40, in addition to for DI water and ethanol, by the SPF-LGFMZI with the structure of $L_1/L_2 = 40.7/64.6 \mu\text{m}$. It was observed that the FSR broadens as the RI of the filling liquids increases, as depicted in Fig. 7(f). This trend can also be estimated using (3), the optical path of liquid-core approaches to that of the cladding, allowing for a significantly high FSR. Specifically, the FSR can exceed 520 nm when utilizing Cargille liquids with $n_D = 1.4$. Furthermore, upon examining the interference spectra of different liquids, it was found that the ER exhibited varying depths due to the different RI of the core; for instance, the ER for Cargille liquids with $n_D = 1.40$ recorded a minimum value of only 7.37 dB,

while the ER for ethanol can reach a maximum of around 34.91 dB. This variation can be attributed to the superimposed interference lights by different RI material dispersion of the various liquids. To investigate the thermal effect of the proposed SPF-LGFMZI, the filled liquids with different RIs were tested to evaluate the T-sensitivity and obtain the TOCs of the fillers. The above experimental results can be obtained by analyzing $\Delta\lambda$ in the interference dips. Fig. 8(a)–(e) shows the measured interference spectra with T variation for Cargille liquids ($n_D = 1.30$, 1.35, and 1.40), DI water, and ethanol, respectively. The corresponding experimental T-sensitivities are 3.44, 4.30, 11.93, 1.57, and 7.12 nm/°C, for the Cargille liquids ($n_D = 1.30$, 1.35, and 1.40), DI water, and ethanol, respectively, as plotted in Fig. 8(f). Notably, the sensor filled with the Cargille liquid of $n_D = 1.40$ did not exhibit complete dips in the interference spectrum due to the huge FSR, making it impossible to estimate T-sensitivity by measuring the wavelength dips. However, it can also evaluate the variations of spectral wavelength shifts by observing a fixed

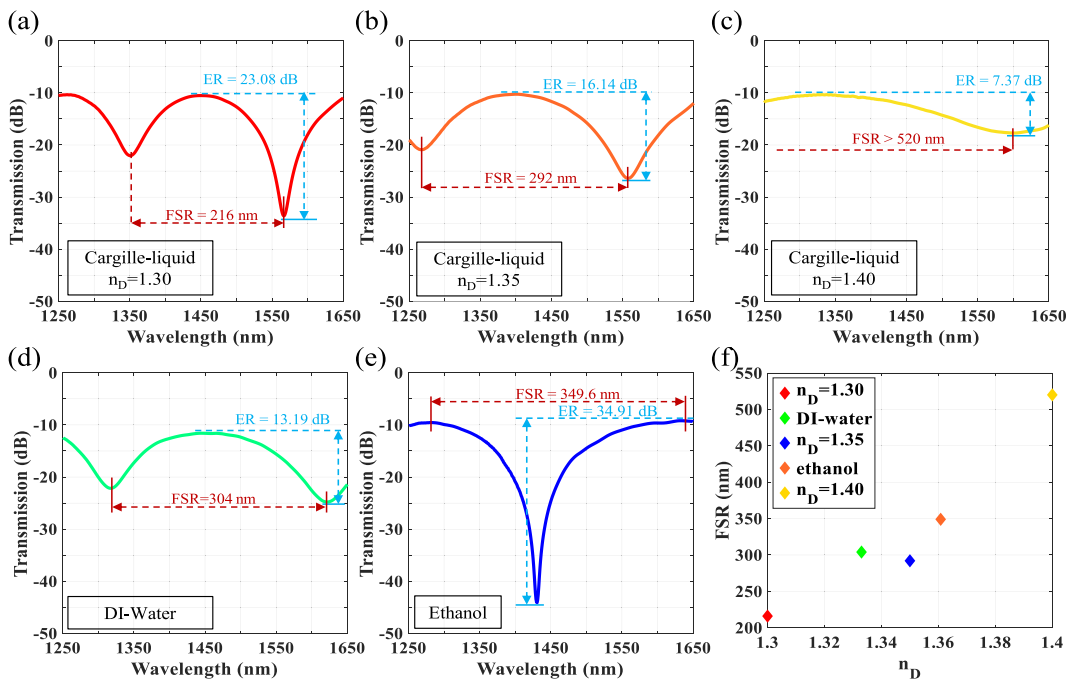


Fig. 7. Interference spectra of the SPF-LGFMZI with the structure of $L_1/L_2 = 40.7/64.6 \mu\text{m}$ corresponding to filling Cargille liquids of n_D = (a) 1.30, (b) 1.35, (c) 1.40, (d) DI water, and (e) ethanol. (f) Relationship between n_D and the FSR for different liquids filled.

TABLE I
COMPARISONS OF THE TOCs FOR DIFFERENT TYPES OF LIQUIDS BETWEEN THE EXPERIMENTAL RESULTS PROPOSED BY THIS STUDY AND THAT OF THE REFERENCE DATA

Liquids	TOC: $k_{co} (\text{ }^{\circ}\text{C}^{-1})$ (measured in the study)	TOC: $k_{co} (\text{ }^{\circ}\text{C}^{-1})$ (reference data)	
DI Water (at 1550 nm)	-9.78×10^{-5}	-7.657×10^{-5}	[25]
Ethanol (at 1550 nm)	-3.19×10^{-4}	-3.688×10^{-4}	[25]
Cargille-Liquid ($n_D = 1.30$)	-2.12×10^{-4}	-2.53×10^{-4}	[29]
Cargille-Liquid ($n_D = 1.35$)	-1.82×10^{-4}	-2.52×10^{-4}	[29]
Cargille-Liquid ($n_D = 1.40$)	-3.20×10^{-4}	-2.94×10^{-4}	[29]

transmission at -11 dB in the interference spectrum covering the 1550-nm wavelength band, as shown in Fig. 8(c). Subsequently, we further estimate the TOCs of the measured liquids by the following TOC equation [27]:

$$k_{co} = \frac{\left(\frac{\lambda'}{\lambda} - 1\right) \cdot (n_{co}^{\text{eff}} - n_{cl}^{\text{eff}}) + n_{co}^{\text{eff}} \cdot k_{cl}}{n_{cl}^{\text{eff}}} \quad (5)$$

where λ and λ' are the corresponding two wavelengths of interference dips at specific T and T' after heating $1 \text{ }^{\circ}\text{C}$, respectively. The obtained TOCs of DI water, ethanol, and Cargille liquids are $-9.78 \text{ }^{\circ}\text{C} \times 10^{-5} \text{ }^{\circ}\text{C}^{-1}$, $-3.19 \text{ }^{\circ}\text{C} \times 10^{-4} \text{ }^{\circ}\text{C}^{-1}$, $-2.12 \text{ }^{\circ}\text{C} \times 10^{-4} \text{ }^{\circ}\text{C}^{-1}$, $-1.82 \text{ }^{\circ}\text{C} \times 10^{-4} \text{ }^{\circ}\text{C}^{-1}$, $-3.20 \text{ }^{\circ}\text{C} \times 10^{-4} \text{ }^{\circ}\text{C}^{-1}$, respectively. The parameters of $n_{cl}^{\text{eff}}(T)$ ($T = 25 \text{ }^{\circ}\text{C}$, $\lambda = 1550 \text{ nm}$) are set at 1.444 for the lowest-order cladding mode and the LG core mode, $n_{co}^{\text{eff}}(T)$ ($T = 25 \text{ }^{\circ}\text{C}$, $\lambda = 1550 \text{ nm}$) would be a complex number that also depends on the RI of filled liquids. Due to the tiny size of the tens of micrometers and the anti-guided characteristics of HCF₂, the estimated values of n_{co}^{eff} are approached as 1.3223, 1.348, 1.2946, 1.3434, and 1.3905 for DI water, ethanol, and

the Cargille liquids with $n_D = 1.30$, 1.35, and 1.40 ($T = 25 \text{ }^{\circ}\text{C}$, $\lambda = 1550 \text{ nm}$). The above-determined TOCs calculated by (5) were further compared with those in the literature, and the results show their consistency, as shown in Table I. Based on the results in Fig. 8(e), the high ER and broadband (over 400 nm) single-wavelength dip of spectra can be obtained. This exceptional performance has great advantages for making broadband measurements to avoid overlapping of the wavelength dips when T varies. We believe that the proposed interferometer sensor presented in this study can be further applied to simultaneous temperature (T) and RI measurements. For simultaneous measurement of the parameters, Lu et al. [30] demonstrated a technique using a feature matrix in a tapered fiber interferometer to simultaneously measure RI and T , allowing for effective decoupling of these two parameters. Later, Jing et al. [31] proposed a method to analyze the RI characteristics of a sensor and eliminate the RI-induced effects on T sensing, further improving measurement accuracy. The approaches offer valuable insights that could be incorporated into future work to enhance the sensing capability of our proposed interferometer.

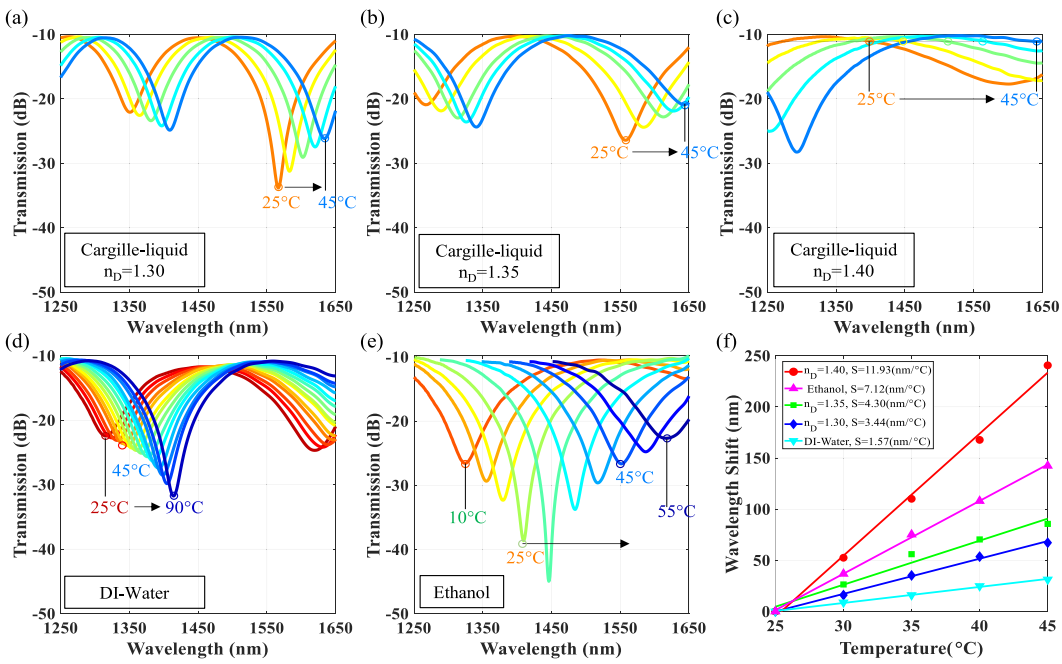


Fig. 8. Interference spectra corresponding to the T variation for Cargille liquids of n_D = (a) 1.30, (b) 1.35, and (c) 1.40. (d) DI water and (e) ethanol. (f) T-sensitivities under different liquids.

IV. CONCLUSION

We have demonstrated an innovative sensing configuration based on an SPF-LGFMZI with an effective filling technique for measuring the TOC and T-sensitivities of liquids. By introducing a side-polished SMF fusion spliced to HCF₁, a microslit is created. HCF₁ connected with the interference section HCF₂ to generate broadband interference spectra with high ER and arbitrary FSR by adjusting the HCF₁ and HCF₂ lengths and the RI of fillers. This designed configuration effectively allows different fillers to access the HCFs through capillary action. Moreover, owing to the different dispersion refractive indices of the filled liquids, we can achieve the desired wavelength interference spectra by selecting the lengths of the HCFs. Additionally, due to the TOC and RI dispersion of the liquid core, the interference spectra of the SPF-LGFMZI exhibit highly modulated characteristics and exceptional T-sensitivity. This configuration provides a stable linear response to thermal effect across a wide wavelength range of 1250–1650 nm. When controlling the lengths of the two HCFs and varying the RI of the liquids, the high ER and broadband single wavelength dip with high sensitivity would be obtained. This unique characteristic has excellent advantages for broadband measurement to avoid the interference wavelength dips from overlapping to make identification impossible. Finally, the proposed fiber sensor can have ultracompact, cost-effective, and single-wavelength dip with broadband-sensitive measurement, high ER performance, and arbitrary FSR. It has the potential to be applied in various fields of sensing technology.

REFERENCES

- [1] C. Meneghini et al., "Determination of ethanol concentration by Raman spectroscopy in liquid-core microstructured optical fiber," *IEEE Sensors J.*, vol. 8, no. 7, pp. 1250–1255, Jul. 2008.
- [2] S. Liu, W. Gao, H. Li, Y. Dong, and H. Zhang, "Liquid-filled simplified hollow-core photonic crystal fiber," *Opt. Laser Technol.*, vol. 64, pp. 140–144, Dec. 2014.
- [3] L. Lv, Q. Liu, and P. Xue, "The sensing characteristics of microstructure-core photonic crystal fiber filled with liquid based on Sagnac interferometer," *Results Phys.*, vol. 18, Sep. 2020, Art. no. 103198.
- [4] J. L. Vilas, J. A. Sanchez-Martin, and E. Bernabeu, "Temperature dependence of birefringence in ethanol-filled suspended core fiber," *Appl. Opt.*, vol. 55, no. 23, p. 6222, Aug. 2016.
- [5] R. Sulzbach, T. Peters, and R. Walser, "Optimal pulse propagation in an inhomogeneously gas-filled hollow-core fiber," *Phys. Rev. A, Gen. Phys.*, vol. 100, no. 1, Jul. 2019, Art. no. 013847.
- [6] K. Naeem, B. H. Kim, B. Kim, and Y. Chung, "High-sensitivity temperature sensor based on a selectively-polymer-filled two-core photonic crystal fiber in-line interferometer," *IEEE Sensors J.*, vol. 15, no. 7, pp. 3998–4003, Jul. 2015.
- [7] C. Markos, G. Antonopoulos, and G. Kakarantzas, "Broadband guidance in a hollow-core photonic crystal fiber with polymer-filled cladding," *IEEE Photon. Technol. Lett.*, vol. 25, no. 20, pp. 2003–2006, Oct. 15, 2013.
- [8] W. Qian, C.-L. Zhao, Y. Wang, C. C. Chan, S. Liu, and W. Jin, "Partially liquid-filled hollow-core photonic crystal fiber polarizer," *Opt. Lett.*, vol. 36, no. 16, p. 3296, Aug. 2011.
- [9] B. Gauvreau et al., "Color-changing and color-tunable photonic bandgap fiber textiles," *Opt. Exp.*, vol. 16, no. 20, pp. 15677–15693, Sep. 2008.
- [10] M. Yang, D. N. Wang, Y. Wang, and C. Liao, "Fiber in-line Mach-Zehnder interferometer constructed by selective infiltration of two air holes in photonic crystal fiber," *Opt. Lett.*, vol. 36, no. 5, pp. 636–638, Feb. 2011.
- [11] J.-M. Hsu, J.-S. Horng, C.-L. Hsu, and C.-L. Lee, "Fiber-optic Michelson interferometer with high sensitivity based on a liquid-filled photonic crystal fiber," *Opt. Commun.*, vol. 331, pp. 348–352, Nov. 2014.
- [12] J. Ma, H. H. Yu, X. Jiang, and D. S. Jiang, "High-performance temperature sensing using a selectively filled solid-core photonic crystal fiber with a central air-bore," *Opt. Exp.*, vol. 25, no. 8, pp. 9406–9415, Apr. 2017.
- [13] X. Ding, S. Liu, M. Wang, N. Chen, and Y. Wang, "Highly sensitive magnetic field sensor using magnetic fluid filled dual-core photonic crystal fiber," *Opt. Laser Technol.*, vol. 175, Aug. 2024, Art. no. 110801.
- [14] Z.-A. Hu, Y.-Q. Huang, A.-P. Luo, H. Cui, Z.-C. Luo, and W.-C. Xu, "Photonic crystal fiber for supporting 26 orbital angular momentum modes," *Opt. Exp.*, vol. 24, no. 15, pp. 17285–17291, Jul. 2016.

- [15] N. Cai, L. Xia, and Y. Wu, "Multiplexing of anti-resonant reflecting optical waveguides for temperature sensing based on quartz capillary," *Opt. Exp.*, vol. 26, no. 25, pp. 33500–33501, Dec. 2018.
- [16] S. Liu, H. Zhang, L. Li, L. Xiong, and P. Shum, "Liquid core fiber interferometer for simultaneous measurement of refractive index and temperature," *IEEE Photon. Technol. Lett.*, vol. 31, no. 2, pp. 189–192, Jan. 15, 2019.
- [17] C.-L. Lee, L.-H. Lee, H.-E. Hwang, and J.-M. Hsu, "Highly sensitive air-gap fiber Fabry-Pérot interferometers based on polymer-filled hollow core fibers," *IEEE Photon. Technol. Lett.*, vol. 24, no. 2, pp. 149–151, Jan. 15, 2012.
- [18] M.-Q. Chen, Y. Zhao, F. Xia, Y. Peng, and R.-J. Tong, "High sensitivity temperature sensor based on fiber air-microbubble Fabry-Pérot interferometer with PDMS-filled hollow-core fiber," *Sens. Actuators A, Phys.*, vol. 275, pp. 60–66, Jun. 2018.
- [19] C.-L. Lee, H.-J. Chang, Y.-W. You, G.-H. Chen, J.-M. Hsu, and J.-S. Horng, "Fiber Fabry-Pérot interferometers based on air-Bubbles/Liquid in hollow core fibers," *IEEE Photon. Technol. Lett.*, vol. 26, no. 8, pp. 749–752, Apr. 15, 2014.
- [20] M. Fuentes-Fuentes, D. May-Arrioja, J. Guzman-Sepulveda, M. Torres-Cisneros, and J. Sánchez-Mondragón, "Highly sensitive liquid core temperature sensor based on multimode interference effects," *Sensors*, vol. 15, no. 10, pp. 26929–26939, Oct. 2015.
- [21] Q. Yu et al., "Temperature compensated magnetic field sensor using magnetic fluid filled exposed core microstructure fiber," *IEEE Trans. Instrum. Meas.*, vol. 71, pp. 1–8, 2022.
- [22] C. L. Lee et al., "Dynamic micro-air-bubble drifted in a liquid core fiber Fabry-Pérot interferometer for directional fiber-optic level meter," *Appl. Phys. Lett.*, vol. 102, no. 19, May 2013, Art. no. 193504.
- [23] J. P. Santos, J. Bierlich, J. Kobelke, and M. S. Ferreira, "A silica capillary-based sensor with access channels for the simultaneous measurement of pressure and temperature," *Photonics*, vol. 10, no. 9, pp. 1029–1043, Sep. 2023.
- [24] C. L. Lee et al., "Microhole-pair hollow core fiber Fabry-Pérot interferometer micromachining by a femtosecond laser," *Sens. Actuators A, Phys.*, vol. 302, pp. 1–5, Feb. 2020.
- [25] C. L. Lee et al., "Dual hollow core fiber-based Fabry-Pérot interferometer for measuring the thermo-optic coefficients of liquids," *Opt. Lett.*, vol. 40, no. 4, pp. 459–462, Feb. 2015.
- [26] Y. Zhao, R.-J. Tong, M.-Q. Chen, and Y. Peng, "Relative humidity sensor based on Vernier effect with QDs-PVA un-fully filled in hollow core fiber," *Sens. Actuators A, Phys.*, vol. 285, pp. 329–337, Jan. 2019.
- [27] C. Lee, W.-R. Zhuo, and T.-K. Liu, "Highly modulated in-fiber Mach-Zehnder interferometer based on an ultracompact leaky-guided liquid core," *Sensors*, vol. 22, no. 3, p. 808, Jan. 2022.
- [28] Y.-H. Lu, R. H. Luo, and C. Lee, "Ultrahigh extinction ratio leaky-guided hollow core fiber Mach-Zehnder interferometer assisted by a large core hollow fiber beam splitter," *Nanomaterials*, vol. 14, no. 18, p. 1494, Sep. 2024.
- [29] Cargille Laboratories. *Refractive Index Liquids*. Accessed: Nov. 12, 2024. [Online]. Available: <https://www.cargille.com/refractive-index-liquids/>
- [30] P. Lu, J. Harris, Y. Xu, Y. Lu, L. Chen, and X. Bao, "Simultaneous refractive index and temperature measurements using a tapered bend-resistant fiber interferometer," *Opt. Lett.*, vol. 37, no. 22, p. 4567, Nov. 2012.
- [31] N. Jing, C. Teng, X. Zhao, and J. Zheng, "Temperature dependence of a refractive index sensor based on a macrobending micro-plastic optical fiber," *Appl. Opt.*, vol. 54, no. 8, p. 1890, Mar. 2015.



Cheng-Ling Lee received the Ph.D. degree in electro-optical engineering from the National Chiao Tung University, Hsinchu, Taiwan, in 2003.

She began her academic career as an Associate Professor with the Department of Electro-Optical Engineering, National United University, Miaoli, Taiwan, from 2004 to 2010. In 2011, she was promoted to a Full Professor. She has authored over 50 peer-reviewed journal articles, focusing on advanced fiber-based devices, optical fiber sensors, and all-fiber interferometers, particularly in developing ultracompact and effective fiber-based devices for various sensing applications.



Chun-Yu Yeh was born in 2003. He received the B.S. degree from the Department of Electro-Optical Engineering, National United University, Miaoli, Taiwan, in 2025. He is about to begin a master's degree from the Institute of Optical Sciences, National Central University, Taoyuan, Taiwan.

His research interests include fiber-based devices, optical fiber sensors, and all-fiber interferometers.



Yu-Xin Jiang was born in 2003. She received the B.S. degree from the Department of Electro-Optical Engineering, National United University, Miaoli, Taiwan, in 2025. She is about to begin a master's degree from the Institute of Lighting and Display Science, National Central University, Taoyuan, Taiwan.

Her research interests include fiber-based devices, optical fiber sensors, and all-fiber interferometers.